Sens Imaging (2017) 18:5
DOI 10.1007/s11220-016-0153-4

ORIGINAL PAPER

On Analytical Solutions to Beam-Hardening

G. Rigaud[1]

Received: 31 October 2016 / Revised: 16 December 2016

Abstract When polychromatic X-rays propagate through a material, for instance in computerized tomography (CT), low energy photons are more attenuated resulting in a "harder" beam. The beam-hardening phenomenon breaks the monochromatic radiation model based on the Radon transform giving rise to artifacts in CT reconstructions to the detriment of visual inspection and automated segmentation algorithms. We propose first a simplified analytic representation for the beam-hardening. Besides providing a general understanding of the phenomenon, this model proposes to invert the beam-hardening effect for homogeneous objects leading to classical monochromatic data. For heterogeneous objects, no analytical reconstruction of the density can be derived without more prior information. However, the beam-hardening is shown to be a smooth operation on the data and thus to preserve the encoding of the singularities of the attenuation map within the data. A microlocal analysis encourages the use of contour extraction methods to solve partially the beam-hardening effect even for heterogeneous objects. The application of both methods, exact analytical solution for homogeneous objects and feature extraction for heterogeneous ones, on real data demonstrates their relevancy and efficiency.

Keywords Beam-hardening · Computerized tomography · Contour reconstruction

This article is part of the Topical Collection on Recent Developments in Sensing and Imaging.

✉ G. Rigaud
rigaud@num.uni-sb.de

[1] Department of Mathematics, Saarland University, 66041 Saarbrücken, Germany

Published online: 09 January 2017

1 Introduction

Computerized tomography (CT) takes advantage of the properties of propagation of high-energy photons—X or γ rays—to image the interior of an illuminated object with a wide range of applications: medical imaging, non-destructive testing, environmental monitoring, etc. For transmission modalities, a source located outside the object of interest emits an isotropic ionizing radiation crossing the medium on straight line paths and then measured by cameras. The recovery of the internal structure of the crossed medium is classically based on the attenuation of the photon beam by the medium, i.e. the loss of intensity of the beam due to the interactions photon/matter. For monochromatic rays, i.e. all emitted photons have the same energy, the Beer–Lambert law provides an analytical model of this phenomenom of attenuation leading to interpret the CT-scan data by the well-known Radon transform [1].

However, the use of mono-energetic sources is not always possible for technical, safety or cost reasons. In medical imaging for instance, soft X-rays are used resulting in a large energy spectrum and then in polychromatic sources. The lineic attenuation coefficient which characterizes the internal structure of the object increases for lower energies. Consequently, during a CT-scan, the photons with lower energies are more attenuated than the higher energy ones. This leads to the phenomenom of beam-hardening and the Beer–Lambert law stops to hold. Thus, the use of standard reconstruction methods, like the Filtered Back-Projection method (FBP), on data affected by beam-hardening can produce harmful artifacts. In medical imaging, a cerebral image can present streak artifacts around the bones which are much more attenuating than the soft tissues [2]. In Industry, the visualization of an homogeneous object, for instance a metal cylinder, can be hindered by cupping artifacts which produce a smooth decreasing of the reconstructed attenuation factor regarding the center of the object [2].

Many methods were proposed in the literature in order to correct either pre or post reconstruction the harmful effect of beam-hardening. A non-exhaustive list is described briefly by Krumm et al. [3]. A first category consists in pre-filtering the X-ray spectrum [4] using for example a Bowtie filter which shapes the X-ray beam in order to equalize it. Some authors proposed also iterative post-correction methods [5, 6]. The third category performs a data calibration with prior beam-hardening distribution via for instance linearization of the beam-hardening [7, 8] or design of effective attenuation coefficient models [9–11]. More recently, beam hardening correction methods that require no prior knowledge of the object composition, X-ray spectrum, and detector response were developed [12].

In this paper, we study the beam-hardening phenomenom in two ways: (i) After an approximation on the dependency of the attenuation factor regarding the energy, we develop a simplified model for the beam-hardening phenomenom. The proposed model requires the knowledge of the spectrum and of the detector response but the X-ray spectrum can be estimated via deterministic models, Monte Carlo simulations, or via transmission measurements [13–15]. Although the model does not provide a general solution to the beam-hardening effect without more prior

information, it depicts the behaviour of beam-hardening by distinguishing precisely a monochromatic part and a polychromatic part in the data. Furthermore, under the proposed model, the beam-hardening effect becomes invertible for homogeneous objects. (ii) Initiated in [16], the second approach follows from the observation that the beam-hardening effect can be interpreted as a smooth function. Thus, exploiting its microlocal properties (cf. [17] for basis of microlocal analysis) we show that the beam-hardening preserves the information encoded in the measurement about the contours of the original attenuation map. We propose therefore to use a regularized contour extraction method [18, 19] in order to recover the contours of the sought-for attenuation map circumventing the beam-hardening effect without prior information.

The paper is organized as follows. Section 2 is dedicated to recall the standard models in CT when the source is monochromatic via the Beer–Lambert law and the X-ray and Radon transforms. In Sect. 3, the beam-hardening is introduced and the proposed model is derived giving rise to a stable solution for homogeneous objects. Section 4 presents the contour extraction approach for solving partially the beam-hardening for homogeneous and heterogeneous objects. In Sect. 5, both approaches are tested on ground truth data. A conclusion ends this paper.

2 Monoenergetic Radiation and Ray Transforms

The variation in intensity for an incident beam of intensity $\Phi_{0,E}$ after crossing the material on length dx is given by

$$d\Phi_E = -f_E \Phi_{0,E} dx$$

with f_E the energy dependant linear attenuation coefficient. For monochromatic radiation (energy E_0), this leads after integration to the well-known Beer–Lambert law which describes the variation of the intensity of a beam crossing a medium of attenuation f_{E_0} along the straight lines L

$$\Phi(L) = \Phi_0 e^{-\int_L f_{E_0}(x)dx}.$$

Denoting by $L(\mathbf{x}, \theta) = \{\mathbf{x} + t\theta, t \in \mathbb{R}^+\}$ the straight line starting at $\mathbf{x} \in \mathbb{R}^3$ with direction $\theta \in S^2$, the measure of the attenuated beam for monochromatic radiation, see Fig. 1, gives the well-known Ray transform $\mathcal{P}$

$$\ln \frac{\Phi_0}{\Phi(\mathbf{x}, \theta)} = \int_0^\infty f_{E_0}(\mathbf{x} + t\theta)dt =: \mathcal{P} f_{E_0}(\mathbf{x}, \theta).$$

In 2D computerized tomography with parallel geometry, the attenuated beam can be understood as the classical Radon transform, *i.e.* the integral of the attenuation along the lines $L(p, \theta) = \{p\theta + t\theta^\perp, t \in \mathbb{R}\}$ with $\theta^\perp \in S^1$ the direction of the line and p its distance to the origin. We define thus the Radon transform $\mathcal{R}$ as

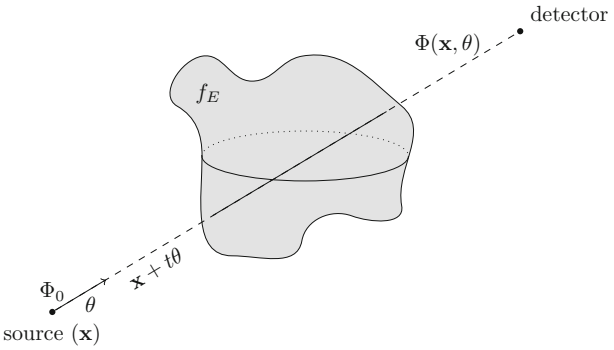

Fig. 1 Propagation of X-rays and geometry of the ray transforms

$$\ln\frac{\Phi_0}{\Phi(p,\theta)} = \int_{-\infty}^{\infty} f_{E_0}(p\theta + t\theta^{\perp})dt =: \mathcal{R}f_{E_0}(p,\theta).$$

The image reconstruction is then classically processed using reconstruction algorithms such as the FBP for $\mathcal{R}$ or the Feldkamp–David–Kress (FDK) algorithm for $\mathcal{P}$ [1].

3 Polychromatic Radiation and Model for Beam-Hardening

When the radiation is polychromatic, the variation in intensity for an incident beam of intensity $\Phi_{0,E}$ after crossing the material on length dx is given by

$$d\Phi_E = -f_E\Phi_{0,E}dx$$

with f_E the energy dependent linear attenuation coefficient. For polychromatic radiation (energy domain $\mathbb{E} = [E_m, E_M]$), the Beer–Lambert law does not hold due to the energy dependency of the attenuation. Integrating over the energy, we obtain the beam-hardening formula,

$$\frac{\Phi(\mathbf{x},\theta)}{\Phi_0} = \int_{\mathbb{E}} T(E)e^{-\int_0^{\infty} f_{E_0}(\mathbf{x}+t\theta)dt}dE = \int_{\mathbb{E}} T(E)e^{-\mathcal{P}f_E(\mathbf{x},\theta)}dE$$

with $T(E)$ the normalized spectrum taking into account the response of the detector. As a consequence, the modeling based on the Radon transform stops to hold for a polychromatic source.

From Stonestrom et al. [20], the dependency regarding the energy of the attenuation coefficient can be approximated by

$$f_E(\mathbf{x}) = E^{-3}f_1(\mathbf{x}) + C(E)f_2(\mathbf{x}) \tag{1}$$

with $C(E)$ the Klein–Nishina function [21] and f_1, f_2 two characteristic maps of the attenuating medium. The first part describes the effect of photoelectric absorption whereas the second one gives the attenuation due to Compton scattering.

In practice, $C(E)$ varies only a little due to the size and position of the X-ray energy range. This is why, to simplify the algebra, we consider in our study $C(E)$ to be a constant a. We take in practice $a := C(E_{max})$. This is validated by Fig. 2 for hard materials such as bones or metals. For low attenuating material, such as brain or water, the approximation does not hold. However, the beam-hardening effect is lower, and in general negligible, for these latter. This approximation is crucial because it enables to rewrite the beam-hardening phenomenon as

$$B(\mathcal{P}f_1, \mathcal{P}f_2)(\mathbf{x}, \theta) := e^{-a\mathcal{P}f_2(\mathbf{x},\theta)} \int_0^\infty T(E) e^{-\mathcal{P}f_1(\mathbf{x},\theta)/E^3} dE$$

and then to separate it into a monochromatic part $e^{-a\mathcal{P}f_2}$ and a polychromatic part, which is denoted by the function

$$P(z) := \int_0^\infty T(E) e^{-z/E^3} dE.$$

In addition, we define for the sequel the data affected by beam-hardening as $g_{BH}(x, \theta) = -\ln B(\mathcal{P}f_1, \mathcal{P}f_2)(x, \theta)$.

3.1 The Proposed Model

The previous decomposition of the function $B(\cdot)$ shows that the strategy to compute a good approximation of the beam-hardening is to design the suited representation for the polychromatic part $P(z)$. Assuming to know the function $T(E)$, it is natural to compute numerically the associated function $P(z)$, see Fig. 3b. We observe that this function is monotone decreasing. Our idea consists hence in approximating $P(z)$ by

$$\tilde{P}(z) = (1 + z/b)^{-c}$$

with b, c constants as depicted in Fig. 3b. The estimation of parameters b and c can be performed using a Gauss–Newton algorithm or a Levenberg–Marquardt algorithm for a more robust convergence [22]. Using a property of the Laplace transform, $\mathcal{L}$, and of the Gamma function, Γ, ([23] p.1110),

$$\mathcal{L}(y^{v-1} e^{-\tau y})(z) = \Gamma(v)(z + \tau)^{-v},$$

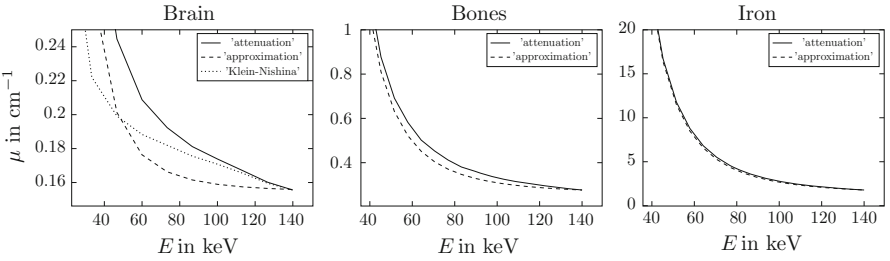

Fig. 2 Approximation of the Klein–Nishina function in the attenuation coefficient for three materials: brain, bone and iron

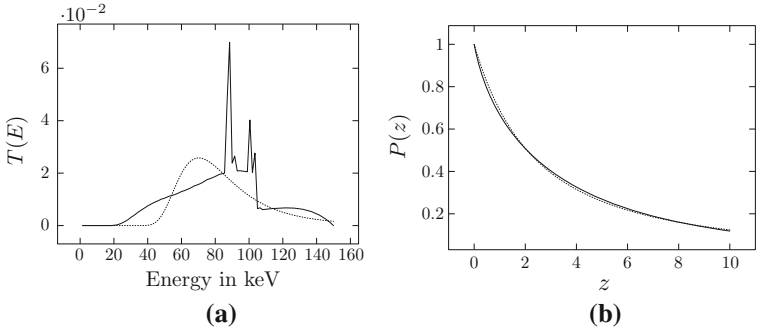

Fig. 3 **a** Spectrum $T(E)$ of a tungsten source at 150 keV in *solid* with the proposed approximation in *dotted*. **b** The corresponding computed polychromatic parts $P(z)$ for the original spectrum in *solid* and for its approximation in *dotted*

we notice that the approximation on $P(z)$ writes

$$\tilde{P}(z) = \frac{b^c}{\Gamma(c)} \mathcal{L}(y^{c-1}e^{-by})(z) = \frac{b^c}{\Gamma(c)} \int_0^\infty y^{c-1}e^{-by}e^{-zy}dy.$$

Making the change of variable $y = E^{-3}$, we obtain that such an approximation on $P(z)$ corresponds to approximate the spectrum by

$$T(E) \approx \frac{3\, b^c}{\Gamma(c)} E^{-3c-1}e^{-b/E^3}.$$

Therefore, the relation between T and P lies on the Laplace transform. Consequently, the continuity of the Laplace transform assures that a good approximation of the spectrum will provide a good approximation of the polychromatic part. However, the exponentially ill-posed nature of the inverse Laplace transform prevents such a transition from P to T. This is why, one shall focus on approximating the polychromatic part and not on the spectrum itself. This becomes clear with Fig. 3a. The approximation of the polychromatic behaviours is accurate in the range of interest although the corresponding spectrum does not fit as well with the original spectrum.

We observe that if there exist constants b, c, ϵ such that

$$\left|P(z) - \tilde{P}(z)\right| \leq \epsilon$$

with $\tilde{P}(z) = (1 + z/b)^{-c}$ for $z \in [0, \max_{\mathbf{x},\theta}(\mathcal{P}f_1)]$, then

$$\left|B(\mathcal{P}f_1, \mathcal{P}f_2) - \tilde{B}(\mathcal{P}f_1, \mathcal{P}f_2)\right| \leq \epsilon$$

with

$$\tilde{B}(\mathcal{P}f_1, \mathcal{P}f_2) = e^{-a\mathcal{P}f_2}(1 + b^{-1}\mathcal{P}f_1)^{-c}. \tag{2}$$

Equation (2) approximates the behaviour of the beam-hardening effect and in particular can be rewritten for the data representation as a sum of a linear part (monochromatic) and a non-linear part (polychromatic),

$$-\ln(\tilde{B}(\mathcal{P}f_1, \mathcal{P}f_2)) = a\mathcal{P}f_2 + c\ln\left(1 + \frac{1}{b}\mathcal{P}f_1\right). \tag{3}$$

Without more prior information about $\mathcal{P}f_1$ and $\mathcal{P}f_2$, this formula does not provide a unique solution to reverse the effect of beam-hardening but enables a simpler interpretation. However, if we consider homogeneous objects, the formula becomes invertible.

3.2 Case of an Homogeneous Object

In the case of homogeneous objects, *i.e.* made of only one material, the functions f_1 and f_2 are constant with respective values $a_1, a_2 > 0$ and Eq. (1) becomes

$$f_E(\mathbf{x}) = (a_1 E^{-3} + a_2 C(E))f(\mathbf{x}) \tag{4}$$

with $f(\mathbf{x}) = 1$ if $\mathbf{x}$ belongs to the support of the object, 0 otherwise. For a homogeneous object, the dependency with the energy of f_E is thus separable from the position $\mathbf{x}$. Putting $\alpha = a_2 a$ and $\beta = a_1/b$, the approximation for the data altered by beam-hardening in Eq. (3) becomes in the homogeneous case

$$-\ln(\tilde{B}(\mathcal{P}f)) = \alpha\mathcal{P}f + c\ln((1 + \beta\mathcal{P}f)) =: \tilde{g}. \tag{5}$$

This analytic model presents the advantages of being invertible. At this purpose, we introduce the W-Lambert function, $W(x)$, (see [24]) as the solution of

$$z(1 + y(z))d_z y(z) = y(z).$$

Solving the Eq. (5), we get an inverse formula for our model of the beam-hardening

$$\mathcal{P}f = \frac{\beta c W\left(\frac{\alpha}{\beta c} e^{\frac{\alpha+\beta\tilde{g}}{\beta c}}\right) - \alpha}{\alpha\beta}.$$

From this model we can therefore correct the effect of beam-hardening and recover the sought-for data $\mathcal{P}f$ in the homogeneous case. By applying the derived inversion formula on the real data g_{BH}, we produce corrected data, noted g_{corr}, with

$$g_{corr} = \frac{\beta c W\left(\frac{\alpha}{\beta c} e^{\frac{\alpha+\beta g_{BH}}{\beta c}}\right) - \alpha}{\alpha\beta}. \tag{6}$$

The image reconstruction consists then to apply a standard reconstruction technique suited to $\mathcal{P}$ on the corrected data g_{corr}. However, we need the stability of the solution g_{corr} regarding the Ray transform $\mathcal{P}f$. This property is given in the following result.

Proposition 1 *If there exist constants* b, c, ϵ *such that*

$$\left|\tilde{P}(z) - P(z)\right| \leq \epsilon$$

with $\tilde{P}(z) = (1 + \beta z)^{-c}$ *for* $z \in [0, \max_{(\mathbf{x},\theta)}(\mathcal{P}f)]$, *then we have the following pointwise estimate*,

$$\forall(\mathbf{x}, \theta), \qquad |\mathcal{P}f(\mathbf{x}, \theta) - g_{corr}(\mathbf{x}, \theta)| \leq (1 + \beta \max_{(\mathbf{x},\theta)}(\mathcal{P}f))^c \frac{\epsilon}{\alpha}.$$

Proof The theorem is a consequence of the mean value theorem. The W-Lambert function satisfies $xW'(x) \leq 1$ leading with h any arbitrary positive constant to

$$d_t W(he^{t/c}) = \frac{1}{c}\ he^{t/c}\ W'(he^{t/c}) \leq \frac{1}{c}.$$

Hence, the mean value theorem leads $\forall(\mathbf{x}, \theta)$ to

$$|\mathcal{P}f(\mathbf{x}, \theta) - \tilde{\mathcal{P}}f(\mathbf{x}, \theta)| \leq \frac{1}{\alpha}|g_{BH} - g|(\mathbf{x}, \theta) = \frac{1}{\alpha}\left|\ln \tilde{P}(\mathcal{P}f) - \ln P(\mathcal{P}f)\right|(\mathbf{x}, \theta).$$

Since the object is bounded, the derivative of the ln-function is bounded by $(1 + \beta \max_{(\mathbf{x},\theta)}(\mathcal{P}f))^c$ which gives the result by applying the mean value theorem.

The approach is implemented and tested on ground truth data in Sect. 5. Furthermore, the results of this section are by analogy the same for the Radon transform $\mathcal{R}$ in 2D. □

4 A Contour Extraction Solution

In this section, we develop a second way to circumvent the beam-hardening effect from the data altered by beam-hardening. The idea is to exploit the smoothness of the function B to show that it preserves the contours. In 3D, more precisely in cone-beam CT, one is confronted with the problem of limited data due to the inconvenience to fulfill the Tuy–Kirilov condition for the source curve [25]. This produces artifacts which can interfer for our study. This is why we consider below the 2D case only and the Radon transform, $\mathcal{R}$. The analysis for the 3D case for complete or incomplete data could be of interest for future works.

4.1 Singular Support and Radon Transform

We define the singular support of a distribution f, noted sing supp f, as the smallest closed set in the complement of which f is a C^∞-function. In imaging applications, this corresponds typically to the contours of the object.

Theorem 1 *Let* $u : (0, \infty) \to \mathbb{R}$ *be smooth and surjective and* $\forall x \in (0, \infty)$, $u'(x) > 0$. *Let* $f : \mathbb{R}^n \to (0, \infty)$ *be in* $L^1_{loc}(\mathbb{R}^n)$. *Then* sing supp $(u \circ f) =$ sing supp f.

Proof We show sing supp $(u \circ f) \subset$ sing supp f and then use the fact that the same is true for $u^{-1} \circ (u \circ f)$ since u^{-1} is smooth by the Inverse Function Theorem.

Let $x_0 \in \mathbb{R}^n$ and assume $x_0 \notin$ sing supp f. Then, there is a neighborhood U of x_0 such that $f : U \to (0, \infty)$ is smooth. Now, since u is smooth, $u \circ f$ is also smooth on U. Therefore, sing supp $(u \circ f) \subset$ sing supp f. □

Theorem 2 *Let* f *be a piecewise smooth function. Then, the mapping between* sing supp f and sing supp $\mathcal{R}f$, namely the Legendre transform $\mathfrak{L}$, *is an involution and* sing supp f *is uniquely determined by* sing supp $\mathcal{R}f$ *and vice versa.*

Proof See [26, Section 4.3]. □

Theorem 3 *An elliptic pseudo-differential operator* $\mathcal{D}$ *preserves the singular support of distributions*

$$\text{sing supp } \mathcal{D}u = \text{sing supp } u.$$

Proof See [27]. □

4.2 Application to Beam-Hardening

The microlocal analysis of the beam-hardening starts from the following simple result. Assuming $T(E)$ integrable, $E_{min} > 0$ and $0 < z < \infty$,

- $P(z)$ is monotone decreasing with $P'(z) \neq 0$

$$P'(z) = -\int_{\mathbb{E}} \frac{T(E)}{E^3} e^{-z/E^3} dE < 0$$

- $P(z)$ is C^∞

$$|P^{(k)}(z)| = \int_{\mathbb{E}} \frac{T(E)}{E^{3k}} e^{-z/E^3} dE < \infty.$$

This means that $-\ln P(z)$ satisfies the condition over the function u in Theorem 1 and hence that it preserves the singular support of $\mathcal{R}f_1$. We assume f_1 and f_2 to be piecewise smooth functions with same contours, noted sing supp f, which is clear due to the structure of the materials. We can now invoke Theorem 2 which states that the mapping sending the singular support of a piecewise smooth function into the singular support of its Radon transform is an involution. This result gives first that $\mathcal{R}f_1, \mathcal{R}f_2$ have same singular support, noted $\mathbb{S}$. Since any elliptic pseudo-differential operator, $\mathcal{D}$, preserves the singular support, we have then

$$\text{sing} \quad \text{supp} \quad \mathcal{D}(a\mathcal{R}f_2 - \ln(P(\mathcal{R}f_1))) = \mathbb{S}.$$

A second application of Theorem 2 provides the desired result by applying the adjoint of the Radon transform, $\mathcal{R}^\star$,

$$\text{sing} \quad \text{supp} \quad \mathcal{R}^\star\mathcal{D}(-\ln B(\mathcal{R}f_1, \mathcal{R}f_2)) = \text{sing} \quad \text{supp} \quad f. \tag{7}$$

This result implies that the choice of a pseudo-differential operator $\mathcal{D}$ enabling the extraction of the contours can provide a reconstruction of the contours of the object circumventing the effect of beam-hardening and without prior information. The theory of feature reconstruction developed in [19] proposes from the problem $\mathcal{R}f = g$ to reconstruct not f but Lf with L a feature operator (the gradient ∇ for example) and thus represents the perfect framework for our application. We focus in the sequel on our particular case and give the general scheme to apply the Approximate Inverse for contours on beam-hardening data.

4.3 Approximate Inverse for Contours

In this part, we define the Radon transform as a compact linear operator between two Hilbert spaces X and Y. $\langle,\rangle_X$ and $\langle,\rangle_Y$ are the associated inner products. Let δ_x^γ be linear functionals approximating the delta distribution δ_x. The approximate inverse, see [18, 19], for recovering the contours—via the gradient—intends then to solve the auxiliary problem

$$\mathcal{R}^\star\psi_x^{\nabla,\gamma} = \nabla\delta_x^\gamma$$

in order to get

$$f_\gamma^\nabla(x) = \left\langle \psi_x^{\nabla,\gamma}, \mathcal{R}f \right\rangle_Y = \left\langle \delta_x^\gamma, \nabla f \right\rangle_X$$

where $x \in \mathbb{R}^2$ is a reconstruction point and $\psi_x^{\nabla,\gamma}$ is the regularizing reconstruction kernel. Using the inverse Radon transform [1], the auxiliary problem reads

$$\mathcal{R}^\star\psi_x^{\nabla,\gamma} = L\delta_x^\gamma = (4\pi)^{-1}\mathcal{R}^\star\mathcal{I}^{-1}\mathcal{R}\nabla\delta_x^\gamma$$

with $\mathcal{I}^{-1}$, the Riesz potential. Exploiting the differentiation property of the Radon transform,

$$\mathcal{R}(\nabla f)(p,\theta) = \theta\frac{\partial}{\partial p}\mathcal{R}f(p,\theta),$$

the approximate reconstruction kernel for finding ∇f writes

$$\psi_x^{\nabla,\gamma} = (4\pi)^{-1}\theta\mathcal{I}^{-1}\frac{\partial}{\partial p}\mathcal{R}\delta_x^\gamma.$$

Since $\mathcal{I}^{-1}\frac{\partial}{\partial p}$ is an elliptic pseudo-differential operator, Eq. (7) states that the application of $\psi_x^{\nabla,\gamma}$ on the beam-hardening data, noted g_{BH},

$$f_\gamma^\nabla = \left\langle \psi_x^{\nabla,\gamma}, g_{BH} \right\rangle_Y \tag{8}$$

builds a regularized image preserving the singular support of the sought-for attenuations f_1, f_2.

For the implementation, we choose a Gaussian mollifier,

$$\delta^\gamma(y) = \frac{1}{2\pi\gamma^2} e^{-|y|^2/(2\gamma^2)},$$

hence, see [19],

$$\psi_x^{\nabla,\gamma}(p,\theta) = -\frac{\theta}{\sqrt{2}\pi^2\gamma^3}\left(\frac{s}{\sqrt{2}\gamma} + \left(1 - \frac{s^2}{\gamma^2}\right) D\left(\frac{s}{\sqrt{2}\gamma}\right)\right)\Big|_{s=p-x\cdot\theta}$$

where $D(.)$ denotes the Dawson's integral, $\int_0^s \exp(t^2 - s^2)dt$ (see [28] for the implementation). In parallel with the correction method presented in the previous section, the contour extraction approach is implemented and tested on ground truth data in the next section.

5 Simulation Results

In this section, we present the simulation results from three ground truth sets of data provided by the Fraunhofer Institute for Nondestructive Testing (IZFP). The first and third set of data were computed with a polychromatic tungsten source at 150 keV, see Fig. 3a for the corresponding $T(E)$. For the second dataset, which are real data, the source was a Viscom XT9225-D tube at 180 kV, 200 μA, 1s integration time and without prefilter. The three objects were designed in order to highlight the beam-hardening effect and built as follows:

- The first one is a ring cylinder made of steel, see Fig. 4. It was measured using 1453 detectors and 800 rotation angles. The reconstruction grid is 256×256 after cropping.
- The second one is a manufacturing object made of ceramic, see Fig. 5. It was measured using 2048 detectors and 800 rotation angles. The reconstruction grid is 2048×2048.
- The last one is made of two different materials; the inside cylinder is made of silicium and the outside ring is made of aluminium, and both parts are closely separated with air, see Fig. 6. It was measured using 512 detectors and 200 rotation angles. The reconstruction grid is 512×512.

Figures 4, 5 and 6 depict in (a) the original raw data, in (b) the FBP reconstruction without correction, in (c) the data after correction of the beam-hardening using Eq. (6), in (d) the corresponding FBP reconstruction after correction of the beam-hardening effect, and in (e) the contours extraction applied on the original data using the approximate inverse, Eq. (8). The different objects make apparent the different harmful effects of the beam-hardening, namely the cupping effect—the attenuation

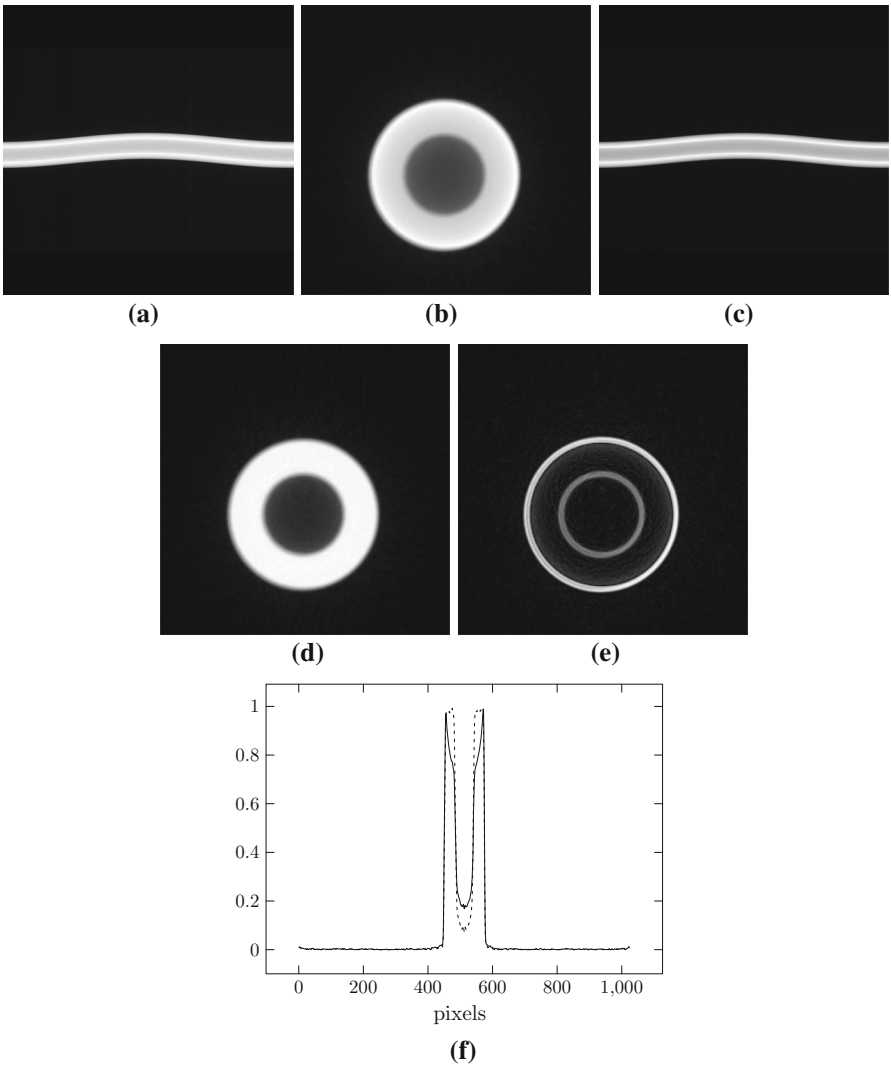

Fig. 4 Steel cylinder: **a** raw data g_{BH}, **b** FBP algorithm applied on data in **a**, **c** corrected data g_{corr} using Eq. (6), **d** FBP algorithm applied on data in **c**, **e** approximate inverse for contours applied on **a**, **f** depicts the central slice in the FBP reconstruction from raw (*solid*) and corrected (*dotted*) data

suffers a loss of intensity regarding the radius—making a homogeneous area look heterogeneous, and the streaks artifacts—in the angular part of the ceramic object. We see that the application of both proposed methods enables to compensate the effect of beam-hardening. The first one in (d) corrects the data according to the proposed model compensating the loss of homogeneity and the streaks artifacts. The third object tests the limits of the method since the object is slightly heterogeneous. For the correction we have considered the object homogeneous and made of silicium. We see that even for slightly heterogeneous objects, the method still

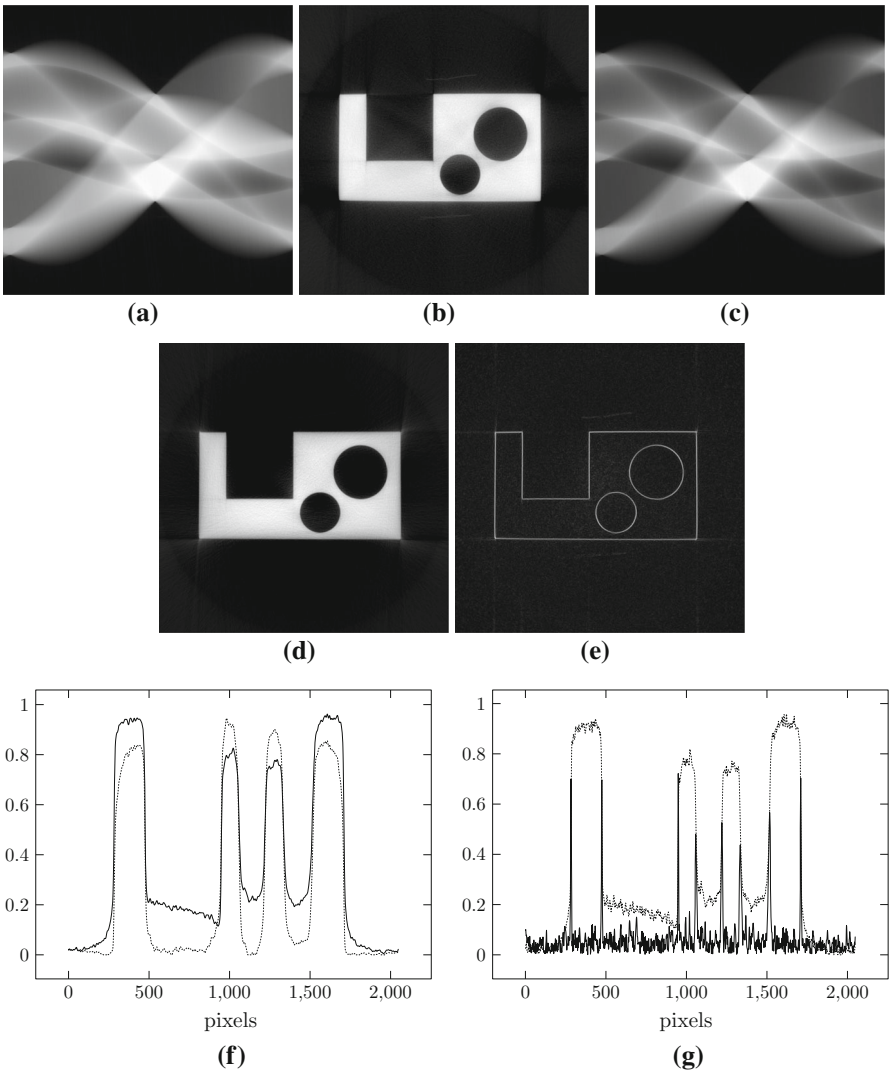

Fig. 5 Ceramic item: **a** raw data g_{BH}, **b** FBP algorithm applied on data in **a**, **c** corrected data g_{corr} using Eq. (6), **d** FBP algorithm applied on data in **c**, **e** Approximate inverse for contours applied on **a**, **f** depicts the central slice in the FBP reconstruction from raw (*solid*) and corrected (*dotted*) data, **g** displays the central slide of the reconstruction using the approximate inverse for contours (*solid*) in comparison with the non-corrected reconstruction (*dotted*)

performs a good correction of the beam-hardening phenomenom, see also (f) for a comparison on the reconstructions on raw and corrected data via a plot of the central slice. In (e), the contour extraction is performed on the raw data exploiting the smoothness properties of the beam-hardening phenomenom. Without correction or compensation, the contours of the different test objects are sharp. In particular, Figs. 5g and 6g testify the efficiency of the contour extraction method on more

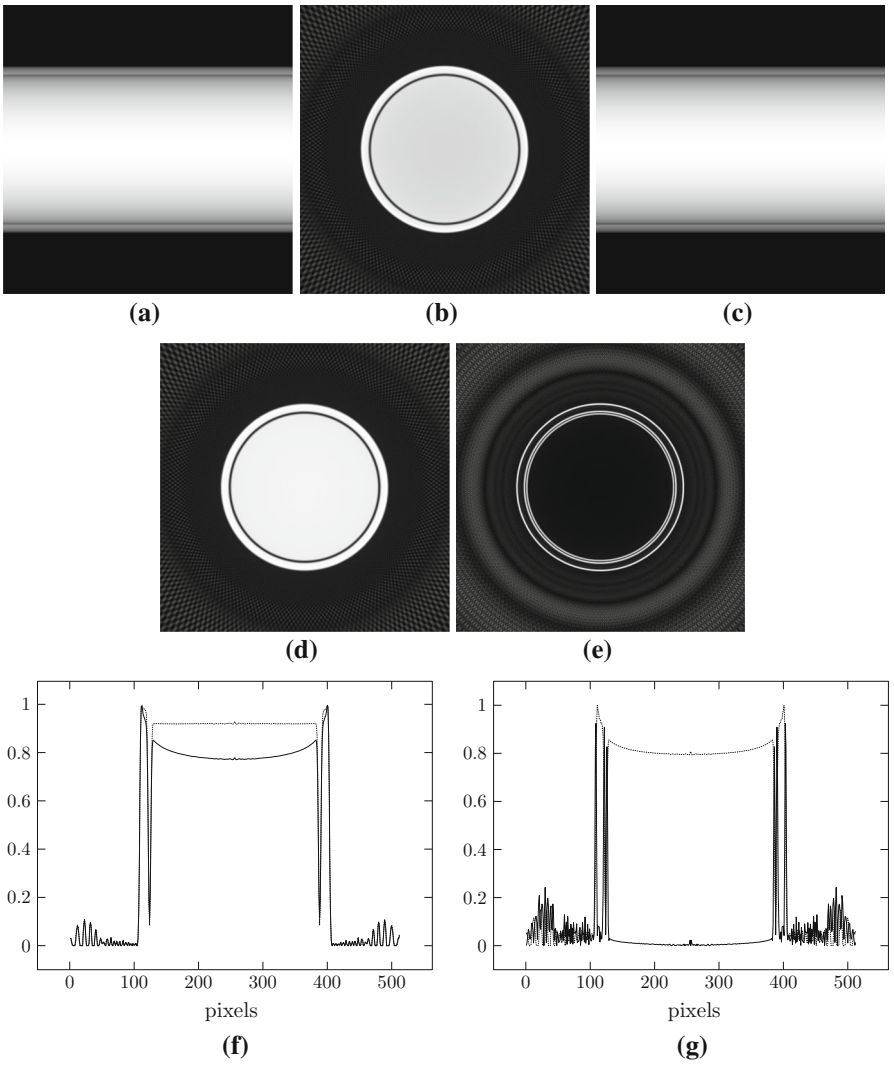

Fig. 6 Aluminium-Silicium cylinder: **a** raw data g_{BH}, **b** FBP algorithm applied on data in **a**, **c** corrected data g_{corr} using Eq. (6), **d** FBP algorithm applied on data in **c**, **e** approximate inverse for contours applied on **a**, **f** depicts the central slice in the FBP reconstruction from raw (*solid*) and corrected (*dotted*) data, **g** displays the central slide of the reconstruction using the approximate inverse for contours (*solid*) in comparison with the non-corrected reconstruction (*dotted*)

complex objects in order to determine precisely the location of the jumps. This can be of particular interest in dimensioning. Finally Fig. 7 show the fidelity of our model with the original data by comparing the polychromatic part, namely $-\ln P(z)$, in the raw data (dotted)—the prior monochromatic part being cut off—taking for z the repartition of the intensity in the data itself with the proposed model (solid). This confirms the use of such a model for the interpretation of the beam-hardening phenomenom.

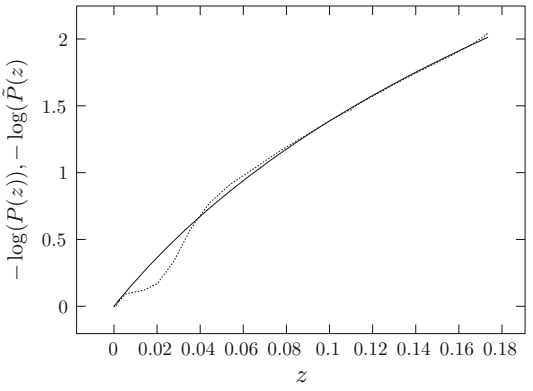

(a)

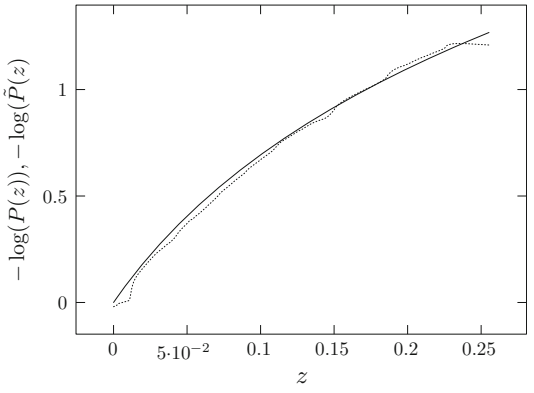

(b)

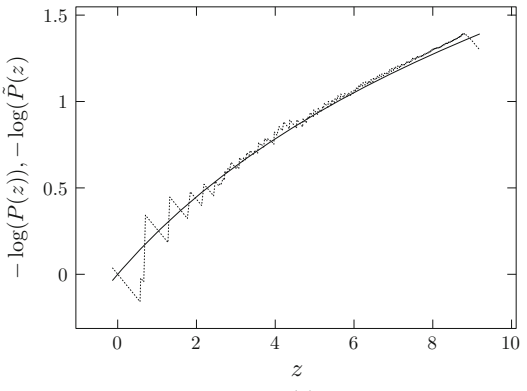

(c)

Fig. 7 **a** (resp. **b**, **c**) compares the polychromatic part in the data (*dotted*) with the considered model $-\log(\tilde{P}(z))$ (*solid*) for the steel cylinder Fig. 4 (resp. the ceramic item Fig. 5 and the aluminium-silicium cylinder Fig. 6)

6 Conclusion

In this paper, we have proposed a novel model for the beam-hardening effect in CT. For homogeneous (or even slightly heterogeneous) objects, the beam-hardening reveals to be analytically invertible and we have provided a pointwise estimate for

the stability of the solution. The application of the method on ground truth data shows the efficiency and the relevancy of the method for understanding and compensating the beam-hardening harmful artifacts for homogeneous objects. However, for the heterogeneous case, the issue of analytically inverting the beam-hardening remains open. Therefore, we have proposed to combine the smoothing property of the beam-hardening function with the microlocal properties of the Radon transform in order to show how the phenomenom preserves the contours of the object. The use of a suitable contour extraction method, the approximate inverse, gives accurate reconstructions of the contours reducing the numerous artifacts. Such an approach is of interest when one needs to measure the dimensions inside the objects. For future works, we intend to develop this last approach for the 3D cone-beam case.

Acknowledgements The author would like to thank Alfred Louis for initiating him to the topic as well as the IZFP for the data. This work was supported by Deutsche Forschungsgemeinschaft under Grant RI 2772/1-1.

References

1. Natterer, F. (2001). *The mathematics of computerized tomography classics in mathematics*. New York: Society for Industrial and Applied Mathematics.
2. Boas, F. E., & Fleischmann, D. (2012). CT artifacts: Causes and reduction techniques. *Imaging in Medicine*, *4*(2), 229–240.
3. Krumm, M., Kasperl, S., & Franz, M. (2008). Reducing non-linear artifacts of multi-material objects in industrial 3D computed tomography. *NDT & E International*, *41*, 242–251.
4. Ding, G. X., Duggan, D. M., & Coffey, C. W. (2007). Characteristics of kilo-voltage X-ray beams used for cone-beam computed tomography in radiation therapy. *Physics in Medicine and Biology*, *52*, 1595–1615.
5. De Man, B., Nuyts, J., Dupont, P., Marchal, G., & Suetens, P. (2001). An iterative maximum-likelihood polychromatic algorithm for CT. *IEEE Transactions on Medical Imaging*, *20*(10), 999–1008.
6. Nalcioglu, O., & Lou, R. Y. (1979). Post-reconstruction method for beam hardening in computerised tomography. *Physics in Medicine and Biology*, *24*(2), 330–340.
7. Rasoulpour, N., Kamali-Asl, A., & Hemmati, H. (2015). A new approach for beam-hardening correction based on the local spectrum distributions. *Nuclear Instruments and Methods in Physics Research A*, *794*, 177–184.
8. Herman, G. T. (1979). Correction for beam hardening in computed tomography. *Physics in Medicine and Biology*, *24*(1), 81–106.
9. Kleinschmidt, C. (1999). Analytical considerations of beam hardening in medical accelerator photon spectrum. *Medical Physics*, *26*, 1995–1999.
10. Alles, J., & Mudde, R. F. (2007). Beam hardening: Analytical considerations of the effective attenuation coefficient of X-ray tomography. *Medical Physics*, *34*(7), 2882–2889.
11. Mathieu, K. B., Kappadath, S. C., White, R. A., Atkinson, E. N., & Cody, D. D. (2011). An empirical model of diagnostic X-ray attenuation under narrow-beam geometry. *Medical Physics*, *38*(8), 4546–4555.
12. Barbant, L., Pauwels, E., Dierick, M., Van Loo, D., Boone, M. A., & Van Hoorebeke, L. (2012). A novel beam hardening correction method requiring no prior knowledge incorporated in an iterative reconstruction algorithm. *NDT & E International*, *51*, 68–73.
13. Poludniowski, G., Landry, G., DeBlois, F., Evans, P. M., & Verhaege, F. (2008). SpekCalc: A program to calculate photon spectra from tungsten anode X-ray tubes. *Physics in Medicine and Biology*, *54*, 433–438.

14. Sidky, E., Yu, L., Pan, X., Zou, Y., & Vannier, M. (2005). A robust method of X-ray source spectrum estimation from transmission measurements: Demonstrated on computer simulated, scatter-free transmission data. *Journal of Applied Physics*, *97*, 124701–124711.
15. Duan, X., Wang, J., Yu, L., Leng, S., & McCollough, C. H. (2011). CT scanner X-ray spectrum estimation from transmission measurements. *Medical Physics*, *38*(2), 993–997.
16. Hahn, B., Louis, A. K., Maisl, M., & Schorr, C. (2013). Combined reconstruction and edge detection in dimensioning. *Measurement Science and Technology*, *24*, 125601.
17. Hörmander, L. (1983). *The analysis of linear partial differential operators*. New York: Springer.
18. Louis, A. K. (2008). Combining image reconstruction and image analysis with an application to 2D—tomography. *SIAM Journal of Imaging Sciences*, *1*, 188–208.
19. Louis, A. (2011). Feature reconstruction in inverse problems. *Inverse Problems*, *27*, 065010.
20. Stonestrom, J. P., Alvarez, R. E., & Macovski, A. (1981). A framework for spectral artifact corrections in X-ray CT. *IEEE Transactions on Biomedical Engineering 2.BME*, *28*, 128–141.
21. Klein, O., & Nishina, Y. (1929). Über die Streuung von Strahlung durch freie Elektronen nach der neuen relativistischen Quantendynamik von Dirac. *Zeitschrift für Physik*, *52*(11–12), 853–869.
22. Marquardt, D. (1963). An algorithm for least-squares estimation of nonlinear parameters. *SIAM Journal on Applied Mathematics*, *11*(2), 431–441.
23. Gradshteyn, I. S., & Ryzhik, I. M. (1964). *Table of Integrals, Series, and Products*. Salt Lake City: Academic Press.
24. Corless, R. M., Gonnet, G. H., Hare, D. E. G., Jeffrey, D. J., & Knuth, D. E. (1996). On the Lambert W function. *Advances in Computational Mathematics*, *5*, 329–359.
25. Tuy, H. K. (1983). An inversion formula for cone-beam reconstruction. *SIAM Journal on Applied Mathematics*, *43*, 546–552.
26. Ramm, A. G., & Katsevich, A. (1999). *The Radon transform and local tomography*. Boca Raton: CRC Press.
27. Treves, F. (1980). *Inrtoduction to pseudodifferential and Fourier integral operators*. New York: Plenum Press, The University Series in Mathematics.
28. Cody, W. J., Paciorek, K. A., & Thacher, H. C. (1970). Chebyshev approximations for Dawson's integral. *Mathematics of Computation*, *24*, 171–178.